Fossilized cell structures identify an ancient origin for the teleost whole-genome duplication

Donald Davesne[a,b,c,1] [ID], Matt Friedman[d,e] [ID], Armin D. Schmitt[a,f] [ID], Vincent Fernandez[g,h] [ID], Giorgio Carnevale[i], Per E. Ahlberg[j] [ID], Sophie Sanchez[g,j] [ID], and Roger B. J. Benson[a,1] [ID]

[a]Department of Earth Sciences, University of Oxford, OX1 3AN Oxford, United Kingdom; [b]Institut de Systématique, Évolution, Biodiversité, UMR 7205, Muséum national d'Histoire naturelle, 75005 Paris, France; [c]Museum für Naturkunde, Leibniz-Institut für Evolutions- und Biodiversitätsforschung, 10115 Berlin, Germany; [d]Museum of Paleontology, University of Michigan, 48109 Ann Arbor, MI; [e]Department of Earth and Environmental Sciences, University of Michigan, 48109 Ann Arbor, MI; [f]Department of Earth Sciences, University of Cambridge, CB2 3EQ Cambridge, United Kingdom; [g]European Synchrotron Radiation Facility, 38000 Grenoble, France; [h]Imaging and Analysis Centre, Natural History Museum, SW7 5BD London, United Kingdom; [i]Dipartimento di Scienze della Terra, Università degli Studi di Torino, 10125 Turin, Italy; and [j]Subdepartment of Evolution and Development, Department of Organismal Biology, Uppsala University, 752 36 Uppsala, Sweden

Teleost fishes comprise one-half of all vertebrate species and possess a duplicated genome. This whole-genome duplication (WGD) occurred on the teleost stem lineage in an ancient common ancestor of all living teleosts and is hypothesized as a trigger of their exceptional evolutionary radiation. Genomic and phylogenetic data indicate that WGD occurred in the Mesozoic after the divergence of teleosts from their closest living relatives but before the origin of the extant teleost groups. However, these approaches cannot pinpoint WGD among the many extinct groups that populate this 50- to 100-million-y lineage, preventing tests of the evolutionary effects of WGD. We infer patterns of genome size evolution in fossil stem-group teleosts using high-resolution synchrotron X-ray tomography to measure the bone cell volumes, which correlate with genome size in living species. Our findings indicate that WGD occurred very early on the teleost stem lineage and that all extinct stem-group teleosts known so far possessed duplicated genomes. WGD therefore predates both the origin of proposed key innovations of the teleost skeleton and the onset of substantial morphological diversification in the clade. Moreover, the early occurrence of WGD allowed considerable time for post-duplication reorganization prior to the origin of the teleost crown group. This suggests at most an indirect link between WGD and evolutionary success, with broad implications for the relationship between genomic architecture and large-scale evolutionary patterns in the vertebrate Tree of Life.

genome duplication | genome evolution | osteocytes | teleostei | paleogenomics

Whole-genome duplication (WGD) has occurred independently in multiple lineages of plants, fungi, and animals (1–3). This represents a major change to genomic architecture, with hypothesized impacts on evolutionary diversification (4, 5) caused by the origin of new gene functions from duplicate copies, expanding the genetic toolbox available for evolutionary "tinkering" (6). However, despite its mechanistic plausibility, this hypothesis is so far supported by only limited and contradictory empirical evidence (7–10). Teleost fishes—comprising more than one-half of modern vertebrates—are a key example, with their spectacular variety of form and kind (ranging from eels to seahorses) often viewed as prima facie evidence for the role of WGD in triggering evolutionary diversification (6, 11). Teleosts also show an incredible diversity of genome biology, demonstrating particularly high rates of evolution of protein-coding genes (12) and noncoding elements (13), a broad range of genome sizes including the smallest known in vertebrates (14), and multiple polyploid lineages (15).

The genome of all living teleosts derives from an ancient WGD event that occurred before the last common ancestor of modern species (16). Additional duplication events occurred more recently in several teleost subgroups (9, 17) but are not generally

proposed as drivers of diversification (9). Studies of the role of WGD in contributing to teleost diversity so far have analyzed the distribution of species richness among extant lineages and morphometric data for fossil phenotypes, with potentially conflicting results: extant teleosts have high rates of lineage diversification compared to other ray-finned fishes (7), but early fossil members of the teleost crown group do not show increased rates of morphological evolution (18).

Molecular phylogenetic studies indicate that WGD occurred on the teleost stem lineage: after the divergence of teleosts from their extant sister taxon (Holostei) but before the most recent common ancestor of all living teleosts (19, 20). However, these bounds encompass a large phylogenetic diversity of extinct groups that diverged during an interval of 50 to 100 million y, from the initial origin of the teleost total group by the Triassic (21), up to the first appearance of crown-group teleosts in the Late Jurassic (18, 22). Molecular-clock estimates provide only broad constraints on the precise timing of duplication [316 to 226 Ma (23); ~310 Ma (24)] and offer no information on its phylogenetic position on the teleost stem lineage. The imprecision of these estimates and the sometimes-considerable incongruence of

Significance

Some lineages of organisms have undergone major evolutionary radiations, while others have not. Establishing why is a central goal of evolutionary research. Whole-genome duplication (WGD) is often proposed as having caused the spectacular evolutionary radiation of teleost fishes. However, due to the absence of genetic data for fossil species, it has been impossible to pinpoint precisely when WGD occurred during teleost history. We use three-dimensional measurements of fossilized bone cell spaces to estimate genome sizes in extinct species, observing a near doubling of size during earliest teleost ancestry. This suggests that WGD occurred very early, substantially predating the dramatic radiation of teleosts. These findings suggest at most an indirect link between WGD and teleost diversification.

molecular clocks with the teleost fossil record question the reliability of these inferences in the absence of further evidence.

Patterns of genome-size evolution on the teleost stem lineage could provide alternative and independent evidence on the timing and phylogenetic position of the teleost WGD. However, stem lineages, by definition, comprise entirely extinct species that are known only from fossils, for which genomic data are absent. Nevertheless, some information about vertebrate genome size is preserved within fossil bone (25–27). Living organisms show a positive correlation between cell size and genome size (28–30), such that the volumes of bone cell spaces (osteocyte lacunae) allow estimates of genome size. This relationship has been demonstrated in ray-finned fishes, including teleosts, and is predictive

for large-scale variation in genome size (31). The precision of this approach is sufficient for inferring the large change (presumably, doubling) of genome size involved in WGD (31). Here, we use this relationship to trace the evolution of genome size in extinct ray-finned fishes using osteocyte lacuna volumes as a proxy for genome size. Our sample includes a broad range of stem- and crown-group teleosts, providing information on patterns of teleost genome-size evolution during the deep evolutionary history of the teleost total group.

Three-dimensional measurement of fossil bone cell spaces with μm-scale diameters presents considerable technical challenges. We used propagation phase contrast synchrotron radiation X-ray microcomputed tomography (PPC-SRμCT) to address this,
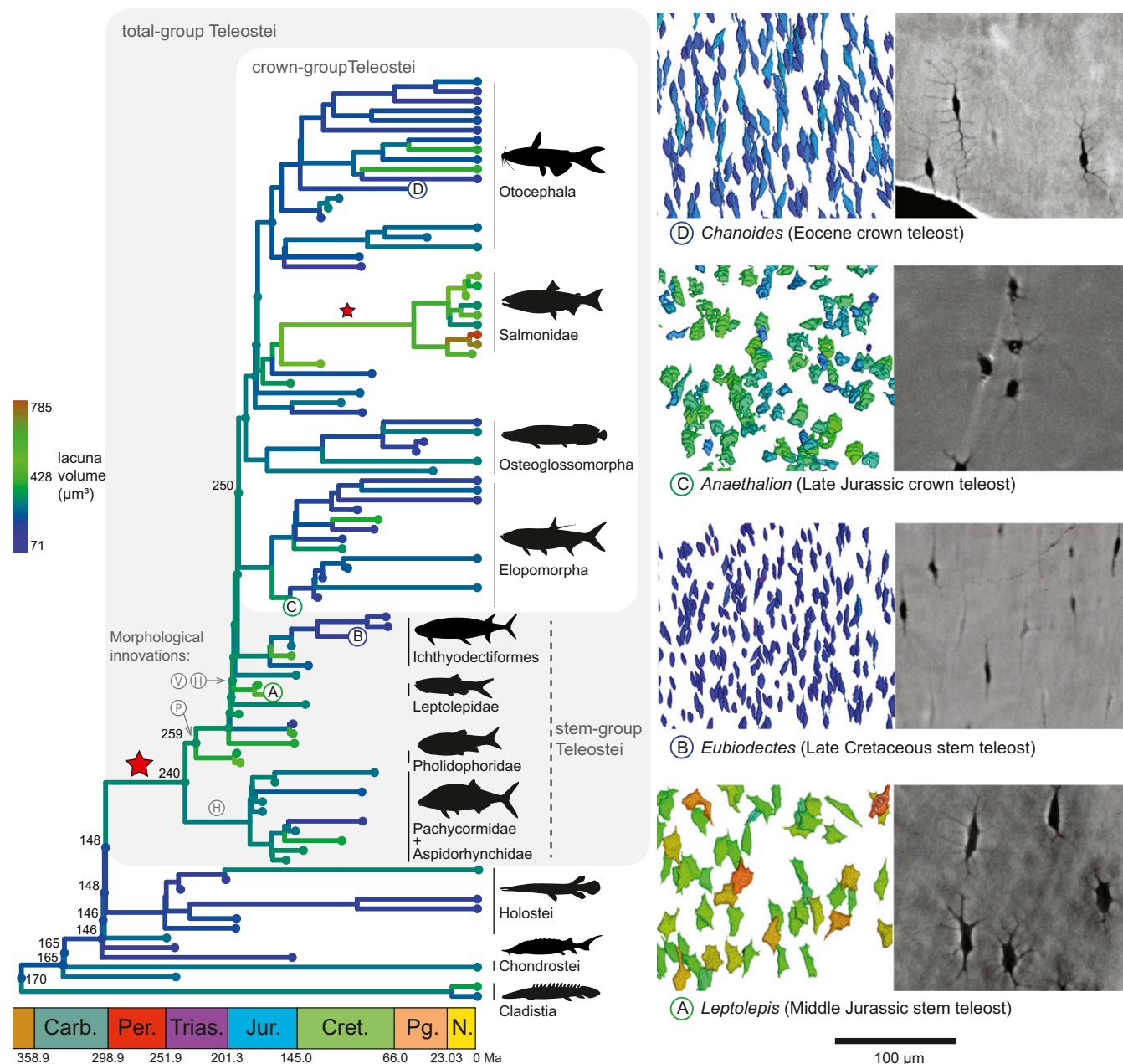
Fig. 1. Evolution of osteocyte lacuna volume in fossil and modern teleosts revealed by synchrotron microtomography. *Left:* timescaled composite phylogeny of actinopterygians with mapped cell-size volumes for fossil and modern lineages. Red stars visualize the inferred occurrences of WGDs: the teleost WGD (large star) and the salmonid-specific WGD (small star). *Right:* renderings of osteocyte lacunae shown for highlighted fossil taxa branching close in time to the inferred teleost-specific WGD (*A* and *C*) and those substantially postdating it (*B* and *D*). Letters correspond to key teleost synapomorphies, mapped to the corresponding node based on morphological phylogeny (35): P, mobile premaxilla; H, homocercal caudal fin; A, vertebral autocentra.

collecting standardized measurements of osteocyte lacuna volumes for 61 fossil ray-finned fish species ranging from 2.5 to 252 million y in age (*SI Appendix,* section I). This fossil evidence is complemented by data from a previous study including 34 modern ray-finned fish species with known genome sizes (31). Our fossil sample includes all major groups of stem-group teleosts, members of both living and extinct lineages within the teleost crown group, and several nonteleost ray-finned fishes. This sample allows us to estimate relative genome sizes in extinct groups, providing information on the absolute timing and specific phylogenetic position of the teleost WGD as well as the timescale of postduplication reductions in genome size (24). Both statistical analysis and qualitative observations demonstrate the effectiveness of lacuna size for inferring large evolutionary increases in genome size: known polyploid lineages such as catostomids and salmonids, which underwent additional rounds of WGD, both show large osteocyte lacuna volumes compared to their close relatives (31).

Results

Our results suggest that WGD occurred early in the teleost stem lineage. Osteocyte lacuna volumes of early- to mid-Mesozoic (Early Jurassic–Early Cretaceous) teleosts overlap with those of extant polyploid taxa and exceed values for most nonpolyploid taxa (Figs. 1 and 2 and *SI Appendix,* Figs. S1–S3). Phylogenetic ancestral trait estimates attribute this to a substantial increase in lacuna volume (from 148 to 240 μm^3) immediately following the split of teleosts from holosteans and therefore before the deepest-known divergences of the teleost total group (Fig. 1). The oldest stem-group teleosts with measurable lacuna volumes in our sample hail from the Early Jurassic (∼195 Ma) and have large lacuna volumes similar to those of recent polyploids such as salmonids and catostomids (Fig. 2). Late Jurassic and Early Cretaceous members of the teleost crown group generally also have large lacunae compared to extant teleosts. In contrast, late Mesozoic and Cenozoic teleosts mostly have lacuna volumes comparable to those of their closest modern relatives (Figs. 1 and 2 and *SI Appendix,* Fig. S1). Osteocyte lacuna volumes therefore decrease through time along the teleost stem-lineage, with further reductions within major lineages of crown teleosts (such as elopomorphs and clupeocephalans) or within some members of the

stem group (such as ichthyodectiforms). Aspects of these patterns of lacuna size evolution are consistent with those inferred from molecular data. Nevertheless, our study provides valuable additional evidence, placing important constraints on the timing and phylogenetic placement of WGD on the extinct teleost stem lineage as a test of its relationship to phenotypic diversification.

Discussion

A large, almost twofold increase in osteocyte sizes at the base of the teleost stem lineage suggests a phylogenetically early occurrence of WGD. Large genome sizes can also occur via other genomic mechanisms such as the accumulation of transposable elements, introns, or tandem repeats (32–34) (e.g., within vertebrates, lungfishes, and salamanders). Nevertheless, the timing, phylogenetic distribution (spanning early members of the teleost stem lineage and their crown group), and observation of subsequent decreases in cell size all suggest that the patterns of genome-size variation inferred here result from WGD and not from other forms of evolutionary genome-size expansion. Furthermore, our previous work has demonstrated that polyploidy provides a strong statistical explanation for large osteocyte size in actinopterygians, on par with genome size (31).

The oldest stem-group teleosts in our sample (*Pholidophoroides* and *Pholidophoropsis*) are of Early Jurassic age. These taxa represent lineages that diverged much earlier from the teleost stem group and therefore constrain the timing of the teleost WGD to no later than the Late Triassic (∼235 Ma) using phylogenetic ancestral state estimation (Fig. 1). Direct sampling of Triassic stem teleosts will provide a further test of this hypothesis (35), but this has not so far been possible despite multiple attempts due to poor preservation of bone microstructure (*SI Appendix,* section II). Our phylogenetically inferred age for the teleost WGD falls within the timeframe estimated by some molecular studies [e.g., 316 to 226 Ma (23)]. The subsequent decrease in lacuna volumes toward the crown and within individual crown-group lineages indicates postduplication genome-size reduction, spanning tens of millions of years. This confirms previous inferences of postduplication genome-size reduction based on clock analysis of paralogous genes, mathematical modeling, and the phylogenetic distribution of genome size in extant
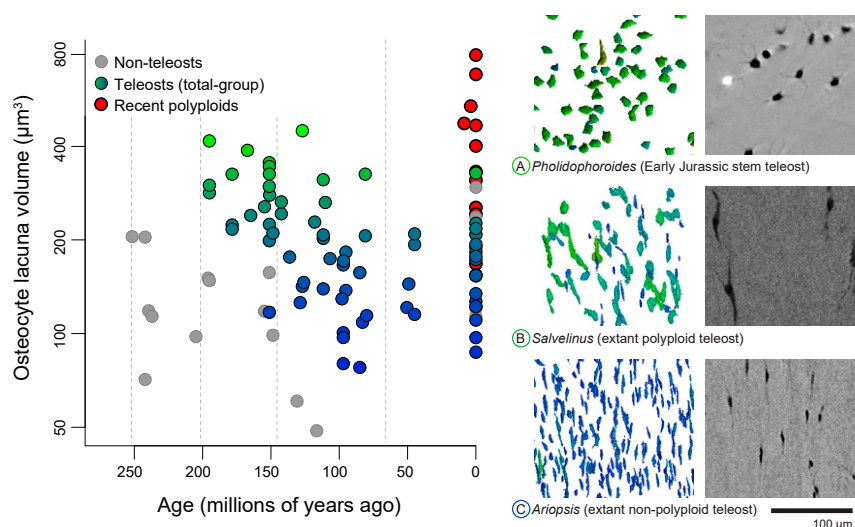
Fig. 2. Evolution of osteocyte lacuna volume in fossil and modern teleosts revealed by synchrotron microtomography, plotted against time. We show cell size in an Early Jurassic stem-group teleost (*A*), within the range of modern polyploid species (exemplified by the salmonid *Salvelinus*; *B*) and indicative of a WGD. A steady decrease in cell size through time is evident in the fossil record and is reflected by the relatively small cells of many extant teleosts, which lack polyploidy events subsequent to the ancestral teleost WGD (e.g., the catfish *Ariopsis*; *C*). Note semilog axes (osteocyte lacuna volume values are log-transformed). Color scale follows Fig. 1.

teleosts (24). Ichthyodectiforms, a long-lived clade of Mesozoic stem teleosts, show a similar pattern of smaller volumes in more recent species compared to earlier ones, providing evidence of parallel reduction in an extinct lineage closely related to the crown (Fig. 1).

Our findings are inconsistent with hypotheses that propose that spectacular evolutionary diversification of teleosts is an immediate consequence of the WGD. Because of the phylogenetically early occurrence of WGD, all currently recognized members of the teleost stem group have inferred duplicate genomes. Therefore, WGD did not coincide with the origin of celebrated teleost functional innovations like the mobile premaxilla, symmetrical caudal fin, and aspects of vertebral geometry implicated in their later evolutionary success (36, 37) (Fig. 1). These traits arose later—conceivably many millions of years after the inferred origin of WGD (35). WGD occurred during or before the Triassic and therefore also predates more general phenotypic diversification, which occurred from the Late Jurassic onwards (38). The earliest known (i.e., Triassic and Early Jurassic) stem teleosts conform to a conservative bodyplan, being small, fusiform fishes with ganoid scales. Quantitative analyses show consistently low levels of morphological diversity for at least ~50 Myr after the origin of the teleost total group (38). The conservative early history of teleosts cannot be attributed to inadequacies of the Triassic record, which yields an abundance of fish fossils (39) including anatomically diverse holosteans (38). The morphological diversity of teleosts increased only gradually in the later stages of the Mesozoic, especially in the Cretaceous with the origin of fundamentally new body plans [e.g., eel like, deep bodied (40, 41)] and amplified by prolific morphological diversification in the early Paleogene (42, 43). Triassic–Early Cretaceous teleosts, including early crown-group taxa, show comparable or lower rates of body-shape evolution than contemporary holosteans (18), which are known to lack duplicated genomes (20). Early teleosts also show delayed patterns of taxonomic and ecological diversification compared to the timing of WGD inferred here: teleosts comprise only a minority of actinopterygian genera in marine and freshwater settings throughout the Triassic (39) and much of the Jurassic (44), even after the origin of their crown group. Only in the Late Jurassic—at least 80 Myr after the WGD—does the taxonomic diversity of teleosts approach or exceed that of other actinopterygians, as evidenced by the marine fossil assemblages of famous *Lagerstätten* like Cerin and Solnhofen (43).

This temporal pattern suggests an alternative hypothesis: that reorganization and integration of genomic architecture after the WGD, and not WGD itself, drove the phenotypic diversification and origin of key morphological traits during later stages of teleost evolution. Consistent with this hypothesis, the 50-Myr interval between the origin of the teleost total group and their observed increase in morphological diversity (38) is similar to the estimated duration of post-WGD genome-size reductions to modern teleost–like levels (20) (Fig. 2). This decrease in genome size is associated with profound changes in genome organization through gene loss, neofunctionalization, and changes in expression.

Because of a recent focus on genomic hypotheses, relatively little attention has been given to alternative explanations for the phenomenal diversity of extant teleosts. However, the temporal incongruence between a Triassic WGD and the late Mesozoic and early Cenozoic events of teleost diversification (18, 38, 43) also demands broader consideration of nongenomic hypotheses. One possibility is that teleosts were the beneficiaries of biotic turnover during major environmental changes of the late Mesozoic. For example, the mid-Cretaceous interval saw substantial environmentally driven alterations to marine ecosystems induced by large igneous province volcanism (45), regional ocean anoxic events (46), and other climatic variations. Among these, the Turonian thermal maximum c. 92 million y ago (47) was a major climate perturbation associated with biotic turnover at all levels of the marine trophic chain (46, 48). The early Late Cretaceous

coincided with a major burst of cladogenesis in marine fishes, the diversity of which is strongly and positively correlated with sea surface temperature during the Jurassic and Cretaceous (44, 49). Although teleosts dominate this mid-Cretaceous radiation, other ray-finned fish groups show similar patterns [e.g., pycnodonts (50)], arguing for a general—rather than clade-specific—mechanism. The Cretaceous concluded 66 million y ago with a major mass extinction event. This induced a large-scale reorganization of aquatic ecosystems, particularly in higher trophic levels of marine environments (51, 52). Paleontological and molecular data indicate substantial morphological diversification among marine teleosts in the early Paleogene (42, 53). This was associated with the colonization of different environments and the refilling of vacated functional roles (54–57) and included short-lived "evolutionary experiments" found alongside familiar living lineages (58, 59). As with the mid-Cretaceous, the early Paleocene represented a "hothouse" period in Earth's climate history, with evidence that higher temperatures might have led to increased fish production in some marine settings (60). Collectively, these observations suggest a role for environmental change and ecosystem reorganization in facilitating the diversification of teleosts, either in addition to or instead of the effects from WGD.

Our results provide direct fossil evidence of phylogenetic placement of the teleost WGD and a more robust window for the timing and consequences of teleost genome duplication. WGD occurred early on the teleost stem lineage, with considerable time for postduplication reorganizations of genomic architecture before the morphological and taxonomic radiation of teleosts. This suggests an indirect and temporally offset link between WGD and evolutionary diversification, if any, and is consistent with genomic studies of recent polyploids among fishes [e.g., salmonids (9)] and vascular plants (10). More broadly, our data demonstrate the potential of the fossil record of cell structures (26) as an independent source of evidence on genomic events that may have underpinned major diversification events, not just in fishes and other vertebrates but also in plants and across the Tree of Life (2, 3).

Materials and Methods

Specimen Collection. Our taxon sample builds on a previous study (31) that collected osteocyte lacuna volumes for 34 species of extant actinopterygians (including 28 teleost species). The present study adds 61 fossil species displaying osteocytic bone (61) to this sample: 8 nonteleost actinopterygians, 26 stem-group teleosts, and 27 crown teleosts. They range from 2.5 (Pliocene) to 252 (Early Triassic) million years in age (*SI Appendix*, section I and Dataset S1). However, no representative of the teleost total group is older than 200 million years (Early Jurassic; *SI Appendix*, section II). As fossil specimens have a higher density than extant ones, capturing a decent signal of transmitted X-ray beam could be challenging should the specimens be too large. Thus, we took small (~1 to 5 mm) bone samples from the fossils, targeting areas that reduced the loss of anatomical information from the specimens (e.g., areas affected by preexisting cracks or broken bone). Since lacunae vary in volume from one bone to another (30, 31), the same skeletal element has to be used consistently across the sample. Therefore, all samples were taken from the dentary bone (lower jaw) as it is found in all target taxa and is often preserved in the fossil record. Moreover, the already-existing dataset of extant actinopterygians (31) used dentary bones for each included species.

Data Acquisition. The data presented in this study were acquired using PPC-SRµCT. Acquisition was performed over the course of three sessions in two synchrotrons: two sessions were done at the ID19 beamline of the European Synchrotron Radiation Facility, and the remaining session was done at the I13-2 Diamond Manchester Imaging beamline of the Diamond Light Source. The setups on the two beamlines were generally similar, the main difference being that much higher energies were available at the ID19 beamline (up to 112 keV in this study) compared to I13-2 beamline (here, 21.39 keV). Both setups produced high-resolution data, with recorded voxel sizes of 0.357 µm at the I13-2 beamline and near 0.7 µm at the ID19 beamline. A voxel size of 0.7 µm or smaller is empirically adequate for imaging osteocyte lacunae (31, 62–64). Detailed information on the synchrotron experimental setups is found in *SI Appendix*, section II and Dataset S2. The tomograms (digital "slices")

obtained from our specimens were processed with the software VGSTUDIO MAX version 3.0 and 3.1 (Volume Graphics) to segment osteocyte lacunae from the fossil bone matrix. We used specimen-specific gray-value thresholds to segment osteocyte lacunae from a selected region of interest, focusing on well-defined lacunae from primary bone, excluding objects such as specimen edges, cracks, and abiotic inclusions manually. Gray-value thresholds were selected to ensure that the boundaries of segmented osteocytes coincided with the boundaries of osteocytes in the image volume, attempting to maximize fit of the segmented object to the underlying data. We did not segment the canaliculi that accommodate cytoplasmic projections of the osteocytes, as they were not visible in every tomogram and thus could bias our estimates of the osteocyte lacuna volumes.

We used the "Porosity/Inclusion" module of VGSTUDIO MAX to measure the individual lacuna volumes. This module also provides visualization, coloring lacunae according to their volume with a consistent color range across our sample (Figs. 1 and 2 and *SI Appendix*, Fig. S1). We analyzed median osteocyte volumes computed from the entire population of segmented objects, excluding objects smaller than 25 μm^3, which did not generally represent osteocyte lacunae. The whole protocol followed the one we applied previously for extant actinopterygians (31), allowing us to incorporate extant and fossil samples together in downstream analyses. The complete measurement and positional data for populations of osteocyte lacunae in all specimens analyzed are available in Dryad (65), and our scan image volumes are available on MorphoSource (66).

We used objective quality control criteria to exclude some specimens from the analysis after obtaining PPC-SRμCT tomograms (*SI Appendix*, section I.3). Datasets were excluded based on the following criteria: 1) When the data clearly showed the absence of osteocyte lacunae from the sample, either because the taxon has anosteocytic bone (61, 67) or because osteocytes were not fossilized; 2) When osteocyte lacunae were present but not sufficiently well-resolved to allow an accurate segmenting of the lacunae or measurement of their volume; 3) After segmenting the osteocyte lacunae, we excluded more specimens in which the number of osteocyte lacunae we were able to measure was too small to warrant confident estimates of average size (n < ~50). Prior to the segmentation and measurement, our sample of tomograms included 77 fossil specimens in total representing 71 species and notably included five stem-group teleosts from the Triassic. Of these, 16 specimens were excluded based on quality control criteria (see the *SI Appendix*, sections I.1 and I.2 for the complete list of specimens).

Reference Tree. We used a composite phylogeny based on a consensus of published hypotheses on the interrelationships of fossil actinopterygians and divergence ages inferred from earliest known occurrences in the fossil record (*SI Appendix*, section I.2 and Dataset S1). The framework for extant taxa is a recently published molecular timetree (68) that has the largest species sample and taxonomic coverage of any actinopterygian phylogeny so far

published. Fossil taxa were stitched to the resulting tree using a custom script that makes extensive use of the R package ape version 5.0 (69) and is available in Dryad (65). Fossil age ranges, specifier taxa for their sister clades, and minimum divergence times from those sister clades based on fossil occurrences are available in Dataset S1. Phylogenetic position and age data for the fossil taxa and their divergence times from other species were taken from the most recent available paleontological and stratigraphic information (see *SI Appendix*, section I.2 for the justification of phylogenetic and stratigraphic placement for each species in the sample). Extant terminals were pruned, retaining the 34 extant species for which we measured osteocyte volumes, prior to analysis. The resulting tree is available in *SI Appendix*, Fig. S1 and as Dataset S3.

Data Analysis. To visualize patterns of genome size evolution, we mapped osteocyte lacuna volume (Dataset S4) to our composite phylogeny with branch lengths of units in time, using ancestral character state estimation (70) via the ace function of ape version 5.0 (69). Osteocyte lacuna volume was $\log_{10}$ transformed prior to analysis and is used as a proxy for genome size (31). WGD predicts an approximate doubling of osteocyte size somewhere on the teleost stem lineage.

Data Availability. The SRμCT data (tomograms and 3D reconstructions) generated during this study have been deposited online in MorphoSource: http://www.morphosource.org/projects/0000C1125 (fossil specimens) (66) and http://www.morphosource.org/projects/00000C959 (extant specimens). The median osteocyte lacuna volumes for each specimen volume evolution are available in Dryad and in Dataset S4. The complete volume measurement data for populations of osteocyte lacunae in all specimen analyzed, as well as the custom R script used to build the reference tree and reconstruct osteocyte lacuna volume evolution are available in Dryad (https://doi.org/10.5061/dryad.bcc2fqzcc) (65). All other data files are included in *SI Appendix* and Datasets S1–S4.

1. Y. Van de Peer, S. Maere, A. Meyer, The evolutionary significance of ancient genome duplications. *Nat. Rev. Genet.* **10**, 725–732 (2009).
2. J. W. Clark, P. C. J. Donoghue, Whole-genome duplication and plant macroevolution. *Trends Plant Sci.* **23**, 933–945 (2018).
3. O. Simakov et al., Deeply conserved synteny resolves early events in vertebrate evolution. *Nat. Ecol. Evol.* **4**, 820–830 (2020).
4. S. Ohno, *Evolution by Gene Duplication* (Springer, 1970).
5. K. D. Crow, G. P. Wagner; SMBE Tri-National Young Investigators, What is the role of genome duplication in the evolution of complexity and diversity? *Mol. Biol. Evol.* **23**, 887–892 (2006).
6. S. M. K. Glasauer, S. C. F. Neuhauss, Whole-genome duplication in teleost fishes and its evolutionary consequences. *Mol. Genet. Genomics* **289**, 1045–1060 (2014).
7. F. Santini, L. J. Harmon, G. Carnevale, M. E. Alfaro, Did genome duplication drive the origin of teleosts? A comparative study of diversification in ray-finned fishes? *BMC Evol. Biol.* **9**, 194 (2009).
8. R. Ren et al., Widespread whole genome duplications contribute to genome complexity and species diversity in angiosperms. *Mol. Plant* **11**, 414–428 (2018).
9. D. J. Macqueen, I. A. Johnston, A well-constrained estimate for the timing of the salmonid whole-genome duplication reveals major decoupling from species diversification. *Proc. Biol. Sci.* **281**, 20132881 (2014).
10. I. Mayrose et al., Recently formed polyploid plants diversify at lower rates. *Science* **333**, 1257 (2011).
11. V. Ravi, B. Venkatesh, Rapidly evolving fish genomes and teleost diversity. *Curr. Opin. Genet. Dev.* **18**, 544–550 (2008).
12. V. Ravi, B. Venkatesh, The divergent genomes of teleosts. *Annu. Rev. Anim. Biosci.* **6**, 47–68 (2018).
13. T. Desvignes, J. Sydes, J. Montfort, J. Bobe, J. H. Postlethwait, Evolution after whole genome duplication: Teleost microRNAs. *Mol. Biol. Evol.*, 10.1093/molbev/msab105 (2021).
14. E. M. Smith, T. R. Gregory, Patterns of genome size diversity in the ray-finned fishes. *Hydrobiologia* **625**, 1–25 (2009).
15. R. A. Leggatt, G. K. Iwama, Occurrence of polyploidy in the fishes. *Rev. Fish Biol. Fish.* **13**, 237–246 (2003).
16. A. Amores, et al., Zebrafish *hox* clusters and vertebrate genome evolution. *Science* **282**, 1711–1714 (1998).
17. C. Berthelot et al., The rainbow trout genome provides novel insights into evolution after whole-genome duplication in vertebrates. *Nat. Commun.* **5**, 3657 (2014).
18. J. T. Clarke, G. T. Lloyd, M. Friedman, Little evidence for enhanced phenotypic evolution in early teleosts relative to their living fossil sister group. *Proc. Natl. Acad. Sci. U.S.A.* **113**, 11531–11536 (2016).
19. J. S. Taylor, I. Braasch, T. Frickey, A. Meyer, Y. Van de Peer, Genome duplication, a trait shared by 22000 species of ray-finned fish. *Genome Res.* **13**, 382–390 (2003).
20. I. Braasch et al., The spotted gar genome illuminates vertebrate evolution and facilitates human-teleost comparisons. *Nat. Genet.* **48**, 427–437 (2016).
21. M. Friedman, The early evolution of ray-finned fishes. *Palaeontology* **58**, 213–228 (2015).
22. G. Arratia, "The Jurassic and the early history of teleosts" in *Mesozoic Fishes—Systematics and Paleoecology*, G. Arratia, G. Viohl, Eds. (Verlag Dr. Friedriech Pfeil, 1996), pp. 243–259.
23. I. A. Hurley et al., A new time-scale for ray-finned fish evolution. *Proc. Biol. Sci.* **274**, 489–498 (2007).
24. J. Inoue, Y. Sato, R. Sinclair, K. Tsukamoto, M. Nishida, Rapid genome reshaping by multiple-gene loss after whole-genome duplication in teleost fish suggested by mathematical modeling. *Proc. Natl. Acad. Sci. U.S.A.* **112**, 14918–14923 (2015).
25. C. L. Organ, A. M. Shedlock, A. Meade, M. Pagel, S. V. Edwards, Origin of avian genome size and structure in non-avian dinosaurs. *Nature* **446**, 180–184 (2007).
26. P. C. J. Donoghue, Fossil cells. *Curr. Biol.* **30**, R485–R490 (2020).
27. C. L. Organ, A. Canoville, R. R. Reisz, M. Laurin, Paleogenomic data suggest mammal-like genome size in the ancestral amniote and derived large genome size in amphibians. *J. Evol. Biol.* **24**, 372–380 (2011).
28. T. Cavalier-Smith, Skeletal DNA and the evolution of genome size. *Annu. Rev. Biophys. Bioeng.* **11**, 273–302 (1982).

Davesne et al.
Fossilized cell structures identify an ancient origin for the teleost whole-genome duplication

PNAS | 5 of 6
https://doi.org/10.1073/pnas.2101780118

EVOLUTION

29. E. Olmo, Nucleotype and cell size in vertebrates: A review. *Basic Appl. Histochem.* **27**, 227–256 (1983).

30. M. D. D'Emic, R. B. J. Benson, Measurement, variation, and scaling of osteocyte lacunae: A case study in birds. *Bone* **57**, 300–310 (2013).

31. D. Davesne, A. D. Schmitt, V. Fernandez, R. B. J. Benson, S. Sanchez, Three-dimensional characterization of osteocyte volumes at multiple scales, and its relationship with bone biology and genome evolution in ray-finned fishes. *J. Evol. Biol.* **33**, 808–830 (2020).

32. T. Lefébure *et al.*, Less effective selection leads to larger genomes. *Genome Res.* **27**, 1016–1028 (2017).

33. H. C. Liedtke, D. J. Gower, M. Wilkinson, I. Gomez-Mestre, Macroevolutionary shift in the size of amphibian genomes and the role of life history and climate. *Nat. Ecol. Evol.* **2**, 1792–1799 (2018).

34. A. Kapusta, A. Suh, C. Feschotte, Dynamics of genome size evolution in birds and mammals. *Proc. Natl. Acad. Sci. U.S.A.* **114**, E1460–E1469 (2017).

35. G. Arratia, Morphology, taxonomy, and phylogeny of Triassic pholidophorid fishes (Actinopterygii, Teleostei). *J. Vertebr. Paleontol.* **33**, 1–138 (2013).

36. B. Schaeffer, D. E. Rosen, Major adaptive levels in the evolution of the actinopterygian feeding mechanism. *Am. Zool.* **1**, 187–204 (1961).

37. L. Sallan, Evolution: Spinal innovation enabled by genome duplication. *Curr. Biol.* **30**, R1006–R1008 (2020).

38. J. T. Clarke, M. Friedman, Body-shape diversity in Triassic–Early Cretaceous neopterygian fishes: Sustained holostean disparity and predominantly gradual increases in teleost phenotypic variety. *Paleobiology* **44**, 402–433 (2018).

39. C. Romano *et al.*, Permian-Triassic Osteichthyes (bony fishes): Diversity dynamics and body size evolution. *Biol. Rev. Camb. Philos. Soc.* **91**, 106–147 (2016).

40. J. G. Maisey, *Santana Fossils: An Illustrated Atlas*, J. G. Maisey, Ed. (T.F.H., 1991).

41. P. L. Forey, L. Yi, C. Patterson, C. E. Davies, Fossil fishes from the Cenomanian (Upper Cretaceous) of Namoura, Lebanon. *J. Syst. Palaeontology* **1**, 227–330 (2003).

42. M. Friedman, Explosive morphological diversification of spiny-finned teleost fishes in the aftermath of the end-Cretaceous extinction. *Proc. Biol. Sci.* **277**, 1675–1683 (2010).

43. G. Guinot, L. Cavin, 'Fish' (Actinopterygii and Elasmobranchii) diversification patterns through deep time. *Biol. Rev. Camb. Philos. Soc.* **91**, 950–981 (2016).

44. L. Cavin, P. L. Forey, C. Lécuyer, Correlation between environment and Late Mesozoic ray-finned fish evolution. *Palaeogeogr. Palaeoclimatol. Palaeoecol.* **245**, 353–367 (2007).

45. S. E. Bryan *et al.*, The largest volcanic eruptions on Earth. *Earth Sci. Rev.* **102**, 207–229 (2010).

46. R. M. Leckie, T. J. Bralower, R. Cashman, Oceanic anoxic events and plankton evolution: Biotic response to tectonic forcing during the mid-Cretaceous. *Paleoceanography* **17**, 1–29 (2002).

47. C. Linnert *et al.*, Evidence for global cooling in the Late Cretaceous. *Nat. Commun.* **5**, 4194 (2014).

48. V. Fischer, N. Bardet, R. B. J. Benson, M. S. Arkhangelsky, M. Friedman, Extinction of fish-shaped marine reptiles associated with reduced evolutionary rates and global environmental volatility. *Nat. Commun.* **7**, 10825 (2016).

49. G. Guinot, L. Cavin, Distinct responses of elasmobranchs and ray-finned fishes to long-term global change. *Front. Ecol. Evol.* **7**, 513 (2020).

50. J. J. Cawley *et al.*, Rise and fall of †Pycnodontiformes: Diversity, competition and extinction of a successful fish clade. *Ecol. Evol.* **11**, 1769–1796 (2021).

51. N. Bardet, Extinction events among Mesozoic marine reptiles. *Hist. Biol.* **7**, 313–324 (1994).

52. M. Friedman, Ecomorphological selectivity among marine teleost fishes during the end-Cretaceous extinction. *Proc. Natl. Acad. Sci. U.S.A.* **106**, 5218–5223 (2009).

53. E. C. Sibert, R. D. Norris, New age of fishes initiated by the Cretaceous-Paleogene mass extinction. *Proc. Natl. Acad. Sci. U.S.A.* **112**, 8537–8542 (2015).

54. E. Ribeiro, A. M. Davis, R. A. Rivero-Vega, G. Ortí, R. Betancur-R, Post-Cretaceous bursts of evolution along the benthic-pelagic axis in marine fishes. *Proc. Biol. Sci.* **285**, 20182010 (2018).

55. M. Friedman *et al.*, A phylogenomic framework for pelagiarian fishes (Acanthomorpha: Percomorpha) highlights mosaic radiation in the open ocean. *Proc. Biol. Sci.* **286**, 20191502 (2019).

56. D. R. Bellwood, C. H. R. Goatley, O. Bellwood, The evolution of fishes and corals on reefs: Form, function and interdependence. *Biol. Rev. Camb. Philos. Soc.* **92**, 878–901 (2017).

57. S. A. Price *et al.*, Two waves of colonization straddling the K-Pg boundary formed the modern reef fish fauna. *Proc. Biol. Sci.* **281**, 20140321 (2014).

58. D. Davesne, G. Carnevale, M. Friedman, *Bajaichthys elegans* from the Eocene of Bolca (Italy) and the overlooked morphological diversity of Zeiformes (Teleostei, Acanthomorpha). *Palaeontology* **60**, 255–268 (2017).

59. A. Capobianco *et al.*, Large-bodied sabre-toothed anchovies reveal unanticipated ecological diversity in early Palaeogene teleosts. *R. Soc. Open Sci.* **7**, 192260 (2020).

60. G. L. Britten, E. C. Sibert, Enhanced fish production during a period of extreme global warmth. *Nat. Commun.* **11**, 5636 (2020).

61. D. Davesne *et al.*, The phylogenetic origin and evolution of acellular bone in teleost fishes: Insights into osteocyte function in bone metabolism. *Biol. Rev. Camb. Philos. Soc.* **94**, 1338–1363 (2019).

62. S. Sanchez *et al.*, 3D microstructural architecture of muscle attachments in extant and fossil vertebrates revealed by synchrotron microtomography. *PLoS One* **8**, e56992 (2013).

63. S. Sanchez, P. Tafforeau, P. E. Ahlberg, The humerus of *Eusthenopteron*: A puzzling organization presaging the establishment of tetrapod limb bone marrow. *Proc. Biol. Sci.* **281**, 20140299 (2014).

64. S. Sanchez, P. E. Ahlberg, K. M. Trinajstic, A. Mirone, P. Tafforeau, Three-dimensional synchrotron virtual paleohistology: A new insight into the world of fossil bone microstructures. *Microsc. Microanal.* **18**, 1095–1105 (2012).

65. D. Davesne *et al.*, Data from: Fossilized cell structures identify an ancient origin for the teleost whole-genome duplication. *Dryad* Dataset. https://doi.org/10.5061/dryad.bcc2fqzcc. Deposited 8 July 2021.

66. D. Davesne, R. B. J. Benson, Fossilized cell structures identify an ancient origin for the teleost whole-genome duplication. MorphoSource Dataset. http://www.morphosource.org/projects/0000C1125. Deposited 8 July 2021.

67. D. Davesne, F. J. Meunier, M. Friedman, R. B. J. Benson, O. Otero, Histology of the endothermic opah (*Lampris* sp.) suggests a new structure-function relationship in teleost fish bone. *Biol. Lett.* **14**, 20180270 (2018).

68. D. L. Rabosky *et al.*, An inverse latitudinal gradient in speciation rate for marine fishes. *Nature* **559**, 392–395 (2018).

69. E. Paradis, K. Schliep, ape 5.0: An environment for modern phylogenetics and evolutionary analyses in R. *Bioinformatics* **35**, 526–528 (2019).

70. D. Schluter, T. Price, A. Ø. Mooers, D. Ludwig, Likelihood of ancestor states in adaptive radiation. *Evolution* **51**, 1699–1711 (1997).